Lawrence Berkeley National Laboratory
Lawrence Berkeley National Laboratory

Title
AUGER ELECTRON SPECTROSCOPY

Permalink
https://escholarship.org/uc/item/4tq5d2k6

Author
Somorjai, G.A.

Publication Date
1980-12-01

Peer reviewed

eScholarship.org Powered by the California Digital Library
University of California

LBL-11720
CONF-801238--1

Lawrence Berkeley Laboratory
UNIVERSITY OF CALIFORNIA

Materials & Molecular Research Division

Presented as an invited paper at the EXXON Conference on Surface Science, Linden, NJ, December 4-5, 1980

AUGER ELECTRON SPECTROSCOPY

G.A. Somorjai

December 1980

MASTER

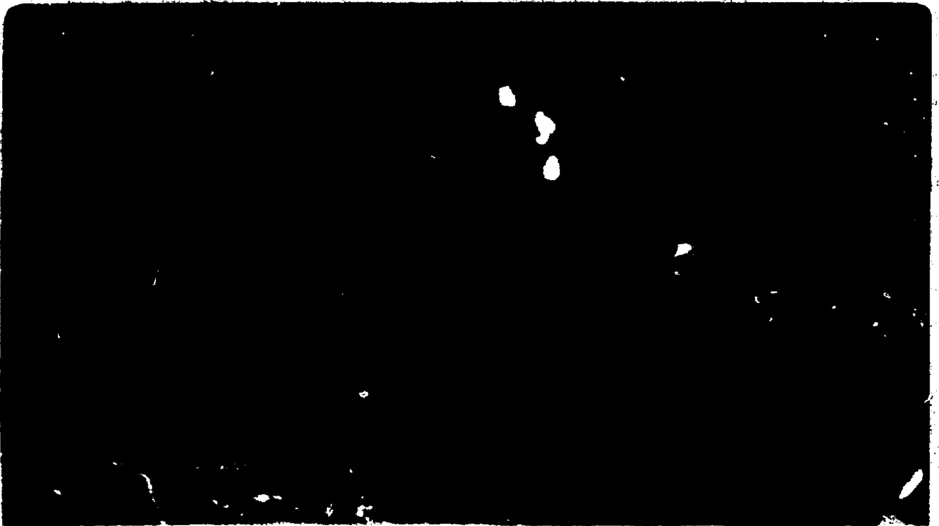

DISTRIBUTION OF THIS DOCUMENT IS UNLIMITED

Prepared for the U.S. Department of Energy under Contract W-7405-ENG-48

LBL 11720

DISCLAIMER

AUGER ELECTRON SPECTROSCOPY

G. A. Somorjai

Materials and Molecular Research Division, Lawrence
Berkeley Laboratory, and Department of Chemistry
University of California, Berkeley, CA 94720 USA

This work was supported by the U.S. Department of Energy under
Contract W-7405-ENG-48.

This manuscript was printed from originals provided by the author.

DISTRIBUTION OF THIS DOCUMENT IS UNLIMITED

The Auger Electron Emission Process

Auger electron spectroscopy (AES) is suitable for studying the composition of solid and liquid surfaces. The sensitivity is about 1% of a monolayer (one monolayer is about 10^{15} atoms/cm^2) and it may be used with relative ease as compared with several other techniques of electron spectroscopy.[1] At present this is the most widespread technique for studies of surface composition. The Auger electron emission occurs in the following manner: when an energetic beam of electrons or X-rays (1000 to 5000 eV) strikes the atoms of a material, electrons, which have binding energies less than the incident beam energy, may be ejected from the inner atomic level. By this process a singly ionized, excited atom is created. The electron vacancy thus formed is filled by de-excitation of electrons from other electron energy states that fill the vacancy. The energy released in the resulting electronic transition can, by electrostatic interaction, be transferred to still another electron in the same atom or in a different atom. If this electron has a binding energy that is less than the energy transferred to it from the de-excitation of the previous process that involves the filling of the deep-lying electron vacancy, it will then be ejected into vacuum, leaving behind a doubly ionized atom. The electron that is ejected as a result of the de-excitation process is called an Auger electron, and its energy is primarily a function of the energy level separations in the atom. These processes are schematically displayed in Figure 1. The creation, detection, and interpretation of this emission process is Auger electron spectroscopy.

A study of the distribution of emitted electrons, N(E) (Figure 2), can yield great amounts of physical information about the type and quantity of atoms present, the electronic structure of the solid, the processes of transport, and relaxation of energetic electrons in a solid, and many other

DISTRIBUTION OF THIS DOCUMENT IS UNLIMITED

phenomena. In addition to the Auger electrons, however, a solid bombarded by an energetic primary electron beam will emit a broad background of electrons which have energies ranging between almost zero and the primary energy. This broad background consists of elastically and inelastically scattered primary electrons, Auger electrons, and secondary electron emission.[2,3] The number of Auger electrons which leave a solid without energy loss is very small compared to the immense background. To enhance this signal the distribution of scattered electrons is usually differentiated electronically.

AES is surface sensitive. Electrons of energies from 50-2000 eV interact strongly with solids. The inelastic mean free paths or escape lengths of low energy electrons in various solids are shown in Figure 3. The values given in the Figure are tabulated from many experimental measurements[4] and, due to the difficulty in measuring them, the values have fairly large uncertainties. Nevertheless, when plotted on a log-log plot, the mean free paths in metals seem to be nearly independent of the type of metal, and depend only upon the energy. The low energy electrons around 50 eV have the minimum escape depth of only about 4 Å, while the escape depths increase gradually with energy above 50 eV to about 30 Å for a 2000 eV electron.

The Auger Electron Spectrometer

Since AES is a surface technique, and since the surfaces of clean solids are very reactive, it is necessary to perform the measurements in an ultrahigh vacuum (UHV) system. There are essentially two types of experimental designs for AES deferring in the detection system that is used. One is the retarding grid Auger analyzer which is of the high pass filter type.[5] It has a rather

low signal-to-noise ratio. The main advantage is that the electron optics of a low energy electron diffraction system (LEED) can also be used for obtaining the Auger spectrum. Thus LEED and Auger measurements can be performed using the same apparatus. The other popular design is called the cylindrical mirror analyzer (CMA) which is of the window filter type that has a higher signal-to-noise ratio.[6,7] One advantage of this type of detector is that it allows one to perform the Auger analysis in a short time (10^{-2} sec), compared to the 1 minute or more required for the retarding grid analyzer. Both of these detectors with Auger electron spectroscopy systems are commercially available.

A retarding field analyzer has four concentric hemispherical wire mesh grids and a hemispherical collector plate concentric with the grids. These elements are biased as shown is Figure 4. The sample is positioned at the center of the five hemispheres. The electron beam is either directed through a drift tube which extends through the grids and collector plate or is incident at a grazing angle from outside the analyzer. The single pass CMA consists of two co-axial cylinders which are biased, as shown in Figure 4. The electron beam is either directed along the axis of the cylinders or it may be incident at a grazing angle.

The electron beam excites the sample and a spectrum of electrons, N(E), are emitted. Auger measurements are made by placing a negative D.C. potential V and a small A.C. modulation, $k\sin(\omega t)$, onto the second and third grids of the RFA or onto the outer cylinder (mirror) of the CMA.

For the RFA only electrons with energy greater than $V(\pm k)$ will pass through the grids and strike the collection plate. The analyzer then acts as a high pass cutoff filter. The CMA on the other hand is a differential detector. Of the electrons passing into the entrance slit of the analyzer only those with a particular small energy range, $E\pm \Delta E$, determined by V and the characteristics of the analyzer will pass through the exit slits. For the CMA, this relationship is approximately $E\pm \Delta E \approx 1.76e(V\pm k)$. This difference in the range of collected energies leads to important differences between the two analyzers.

The purpose of the modulation is to obtain a derivative of the N(E) spectrum. Chang [2] has shown that the collected current, I, can be written as follows:

$$I \approx I_o + \left[I'k + \frac{I'''k^3}{8} + \ldots\right]\sin(\omega t) - \left[\frac{I''k^2}{4} + \frac{I''''k^4}{48} + \ldots\right]\cos(2\omega t) + \ldots \quad (1a)$$

$$\approx I_o + I'k\sin(\omega t) - \frac{I''k^2}{4}\cos(2\omega t) + \ldots \quad (1b)$$

Here the primes refer to differentiation with respect to the D.C. potential V. The second equation approximates the first if the modulation amplitude k is sufficiently small. The value of the frequency of ω to be used is largely unimportant. For the RFA a frequency of around 1000 Hz was used while for the single pass CMA $\omega \approx 6000$ Hz was chosen. Since the CMA is a differential detector it is clear that the collected current is proportional to N(E) so that $I' \approx N'(E)$. With a lock-in amplifier it is possible to phase sensitively detect the component, A_1, of the collected current which has frequency ω. For a CMA it follows

from Eq. 1b that $A_1 \approx kI' \approx kN'(E)$ so it is seen that the derivative of the electron distribution curve can be obtained by detecting the first harmonic of the collected current. Since the RFA is a cut off filter, I' $N(E)$ so it is necessary to detect the component A_2 of frequency 2ω to obtain the $N'(E)$ curve, since $A_2 \approx I''k^2/4 \approx N'(E)k^2/4$. This is the first difference between the two types of analyzers. Note that in both cases the signal depends upon the amplitude of the modulation voltage, k, but for the RFA the signal depends upon k^2 while for the CMA the signal varies linearly with k. The signal can be increased by increasing k, within the limit that k is small enough (compared to the peak width) that higher order terms in Eq. 1a are negligible.

A second and most important difference between the analyzers is that the CMA is much more sensitive than the RFA. This arises from the fact that shot noise is the greatest contributor to the electronic noise, and the shot noise current is proportional to the square root of the collected current. In an RFA a greater current is collected so more noise is obtained for the same amount of signal than for the CMA. This results in the CMA having a signal to noise ratio which is about 100 times larger than that of the RFA. This allows less intense Auger peaks (such as the 2024 eV Au peak) to be more quantitatively studied. This also allows the use of higher scanning speeds and/or lower electron beam currents, and the use of smaller modulation amplitudes. The resolution of the analyzer can be no better than the modulation amplitude so resolution may be limited by the need to use a higher modulation amplitude to see a weak signal. For the RFA used for example (shown in Fig.5)
for the Au-Ag system/the sensitivity needed required the use of 10 V

p-p modulation, while the measurements made with the CMA were performed with a modulation of 2 V p-p. There are many additional factors involved in the resolution of the two types of analyzers which will not be discussed here.

Another important difference is the angle of collection. A CMA collects a cone of electrons at an angle $\theta_o = 42.3° \pm 6°$, which depends upon the geometry of the exit slits.[7] The RFA collects all electrons between the smallest angle which misses the drift tube of the normal electron gun and the outside edge of the analyzer (about 60° for the 4-grid RFA). If there is anglular anisotropy in the Auger emission which varies with alloy composition, crystallite orientation, roughness, heat treatment, the RFA will be sensitive to the effect, but the CMA will be affected. This is a disadvantage of the CMA for quantitative purposes.

The CMA is critically sensitive to the placement of the sample. Small movement of the sample away from the focal point along the line defined by the axis of the analyzer results not only in a shift of the peak position and in peak distortion, but also causes a decrease in the signal intensity to an extent which depends upon the energy. The RFA is not nearly as sensitive to this placement and the sample may be moved several millimeters without noticeable effect. This is no real disadvantage of the CMA since it is possible to place the sample in the correct analysis position by maximizing the measured intensity of the elastic peak with respect to sample placement.

The shape of the Auger spectra obtained from a CMA and RFA are also different. At low energies the RFA accurately shows the large background due to secondary emission. Use of the peak-to-peak height in the derivative spectra as a measure of intensity at low energies is affected by the sloping background. The CMA does not show this sloping background due to the fact that it distorts the spectra at low energies. This distortion is due to the energy-dependent transfer function of the analyzer and the energy dependence of the electron multiplier gain. This distortion is also expected to affect the relation between peak-to-peak height and Auger intensity. The assumption will be made that the distortion is similar for all alloys. Spectra recorded with a CMA and an RFA are given in Fig.5 for comparison.

Qualitative Chemical Analysis by AES

Auger electron spectroscopy finds applications mostly for the qualitative and quantitative analyses of surface composition. A lesser, but equally important, application is for the determination of the oxidation states of surface atoms from changes of Auger peak shapes and from the shifts of Auger emission energies from inner shell excitations.

With the exception of hydrogen and helium, all other elements are detectable by AES. Using this technique, surface segregation of various impurities has been found commonly on most surfaces, Carbon, sulfur, calcium, and oxygen are the most common impurities that segregate at the surface and their removal is essential in many cases. Figure 6 shows the Auger spectra of dirty and cleaned Au-Ag alloy surfaces.[8] Chemical cleaning and ion bombardment are used most frequently to remove the unwanted impurities from the surface. It should be remembered that the bulk of the specimen can be a continuous supplier of impurities to the surface. Therefore, most cleaning treatments only reduce the impurity concentration in the near surface region. Heat treatment of the samples can replenish the surface impurities by diffusion from the bulk. Conversely, heating can dissolve surface impurities in the bulk on account of the increased solubilities at higher temperatures. The qualitative surface chemical analysis by AES has opened up many fields of surface science to definitive studies, including heterogeneous catalysis and corrosion. At present almost every fundamental surface study includes Auger or photoelectron spectroscopy analysis of the surface composition as an integral part of the investigation.

Quantitative Chemical Analysis by AES

By suitable analysis of the experimental data, as well as by the use of suitable reference surfaces, the Auger electron spectroscopy can provide quantitative chemical analysis in addition to elemental composition analysis of the surface. It is possible to separate the surface composition from the composition of layers below the surface by appropriate analysis of the Auger spectral intensities. In this way the surface composition as well as the composition in the near surface region can be obtained.

The Auger peak intensity ratios can be calculated by properly taking into account the attenuation of the emitted Auger electrons by the atomic layers above. By comparing the calculated intensities with those obtained by experiments, quantitative chemical analysis can be performed. Since both the adsorbate and the substrate Auger peak intensities vary as the surface coverage changes, there is enough experimental information in most cases to detect when a monolayer coverage is reached and thus calibrate the amount adsorbed.

A simple technique to utilize the Auger spectrum to determine the coverages and growth mechanisms of deposits will also be described below. This method consists of plotting the Auger peak-to-peak signal intensity from the substrate against the similar signal from the adsorbate. This technique enables one to study the growth of deposits of any adsorbate-substrate system. We apply this method to the calibration of coverage of carbon and oxygen deposited on platinum.

Analysis of Auger Intensities

Auger has principally been used as a means of performing qualitative analysis of surfaces, that is to identify or verify the presence of various atomic species. For this purpose AES is certainly the best of all available techniques. Also of interest is the use of AES as a means of quantitatively analyzing a surface to determine how much of an impurity or alloying component is present. This endeavor has occupied the time and efforts of a growing number of workers in the last eight years and it has been successful.

An understanding of quantitative AES begins with an expression describing the intensity of Auger emission.[9] The current, I_E, of Auger electrons arising from a transition observed at energy E, may be phenomenologically divided up into intensities from each atomic layer in the solid. This description arises naturally from considering flat perfect surfaces of infinite extent. This concept is not as well defined for rough surfaces or small clusters, but in spite of this the results obtained using the perfect surface models can be applied to rough polycrystalline samples as well. The intensity from each layer may be described by dividing the Auger process into the following three steps, 1) excitation, 2) emission , and 3) collection. Each step will now be considered.

The standard means of excitation is by bombardment with electrons of energy E_p and current I_p. For most Auger studies E_p is 2 or 5 keV and I_p is usually 15-50 μA spread over an area of about 1 mm^2. The number of atoms ionized in the ith layer near the surface may be expected to be proportional to

$$\text{ionization events} \sim I_p g_p(\Theta_p, \emptyset_p) \rho_i \sigma_I(E_p) p_i(E_r) r_i(E, E_p) \qquad (2)$$

Here ρ_i is the number of atoms per unit area in the ith layer and the function $g_p(\theta_p, \emptyset_p)$ takes the geometric and anisotropic factors in the excitation into account and depends upon the angles of incidence θ_p and $\emptyset_p$ of the primary beam. σ_I is the cross section for ionization of an atom by electrons of energy E_p. p_i is an energy dependent factor which accounts for the attenuation of the primary beam and r_i is a backscattering factor which takes into account that electrons which have been elastically and inelastically scattered may contribute to the ionization.

The excited region of the solid is penetrated by a beam of electrons incident at fixed angles θ_p and $\emptyset_p$ whose intensity decreases with depth due to inelastic and elastic scattering of the primary beams. This region also contains a plasma of electrons of nearly continuous energies and momentums. The terms $\sigma_p(E_p)p_i(E_p)$ in Eq. B.2 takes account of the ionization by the column of primaries while the general term $r_i(E, E_p)$ takes account of the excitation by the plasma. This backscattering term is very complicated and contains the energy dependence of the ionization cross section of the solid and may be expected to vary with depth.[10,11]

To use Eq. 2 approximations must be employed. Typically it is

assumed that there is no anisotropy in the excitation process. Because of attenuation, the more grazing the incident angle θ_p the more energy will be deposited in the surface region from which Auger electrons can be collected. This suggests the form $g(\theta_p,\phi_p) \sim 1/\cos\theta_p$.[9] In fact experiments have shown that this model is only partly correct.[12] In most experiments done the primary beam is normal to the sample ($\cos\theta_p = 1$) so $g(\theta_p,\phi_p)$ can be taken as unity. Eq. ? may be further simplified by assuming that the primary beam intensity or its ionization capability is independent of depth within the region detected by collecting the Auger electrons. The basis for this assumption is the fact that the escape length of an electron with energy $E_p = 5$ keV is large and the average inelastic collision results in only a small energy loss, leaving the primary electron still energetic enough to efficiently ionize. More importantly, this assumption has been experimentally justified.[13] With these assumptions, Eq. 2 simplifies to the following form:

$$\text{ionization events} \sim I_p \sigma_I(E_p) \rho_i r_i(E,E_p) \quad (3)$$

The emission process, the second step in this scheme, is much simpler, and is given in Eq. 4.

$$\text{probability of emission} \sim P_A q_i(E,\theta) \quad (4)$$

The probability of emission is the product of the probability, P_A, that an ionized atom undergoes an Auger process and emits an electron, and the likelihood $q_i(E,\theta)$ that the Auger electron emitted at an angle θ from layer i will escape the surface without an inelastic collision. P_A is characteristic of the type of atom involved and the energy E of the

Auger transition[14] and is assumed to be independent of angle. The attenuation of the electron is usually assumed to be exponential with a characteristic attenuation depth λ_E which depends upon the energy, so Eq. 4 becomes ,

$$\text{probability of emission} \sim P_A \exp(-(i-1)d/\lambda_E\cos\theta) \qquad (5)$$

Here d is the interlayer spacing of the solid, so an atom in the ith layer is at a depth of $(i-1)d$. If the Auger electron is emitted at an angle θ measured from the surface normal, it must travel through the solid a distance $(i-1)d/\cos\theta$ to escape from the solid.

It is important to note that this form holds only if each layer fully covers the layer below it. This is true in a close packed plane such as in the (111) face of an fcc solid. For the (110) face, the surface consists of ridges and troughs so that the atoms at the bottom of the troughs in the second layer are not attenuated fully by the first layer. This leads to the necessity of applying this model only to close packed planes.

It is also important to note that the model assumes that the surface is atomically flat and smooth. If there is roughness, the emission will be affected. Holloway[15] has studied the effects of roughness on Auger emission and has found that even very slight roughness (root mean square displacement of .28μm) could reduce the Auger intensity by up to 40% depending upon the angle of incidence of the primary beam and the collection angle. He found that the effects of roughness were least when a normally incident primary beam was used.

To obtain the total emission Eq. .5 should be integrated over all angles collected. Eq. .4 assumes that the emission is isotropic and that the emitted electrons are not diffracted or otherwise attenuated anisotropically. Experiments show that this may not be true for single crystals.[12,16] For polycrystalline samples,

the presence of crystals of many orientations should eliminate anisotropies.

Finally the collection process, which is the third step of the emission process adds terms which take into account that the detector intercepts a solid angle Ω and so only collects $\Omega/4\pi$ of the emitted Auger electrons. This fraction is further attenuated by the transmission, T, of the detector. For a CMA only electrons emitted at an angle near $\theta_0 \approx 42.3^\circ$ are collected where θ_0 is measured from the axis of the analyzer. If the sample is mounted so that the sample surface is perpendicular to the axis of the analyzer, then θ in Eq. 3.5 becomes θ_0. For the calculations below, an average value of $\theta_0 = 42.3$ is assumed. For this narrow angle detector the factor $\Omega/4\pi$ derives from integrating Eq. 5 over the angle θ.

Combining the number of ionization events times the probability of emission and collection and summing over all the layers of the pure solid gives Eq. 6 for the intensity I_E^o of an Auger peak at energy E.

$$I_E^o = \sum_{i=1}^{\text{layers}} I_p g_p(\theta_p,\phi_p)\rho_i^o\sigma_I^o(E_p)p_i^o(E_p)r_i^o(E,E_p)P_A^o q_i^o(E,\theta)(\Omega/4\pi)T \qquad (6)$$

Here the superscript "o" denotes values characteristic of a pure solid. Making the assumptions suggested above the expression simplifies to the following expression for the absolute Auger intensity from the pure solids.

$$I_E^o = I_p \sigma_I^o(E_p) P_A^o(\Omega/4\pi) T \sum_{i=1}^{layers} \rho_i^o r_i^o(E,E_p) \exp\left(-\frac{(i-1)d^o}{\lambda_E \cos\theta_o}\right) \quad (7a)$$

$$\equiv k^o(E,\ldots)(a_1^o + a_2^o + a_3^o + \ldots) \quad (7b)$$

where, for convenience, $I_p \sigma_I^o(E_p) P_A^o(\Omega/4\pi)$ is written as $k^o(E,\ldots)$ and $\rho_i^o r_i^o(E,E_p)\exp\left(-\frac{(i-1)d^o}{\lambda_E \cos\theta_o}\right)$ is written as a_i^o. This formula can be applied to alloys if ρ_i^o is replaced by $\rho_i x_i$ where x_i is the atom fraction of the emitting species in the ith layer and ρ_i is now the total number of both types of atoms per unit area. This yields for an alloy the following:

$$I_E = I_p \sigma_I(E_p) P_A(\Omega/4\pi) T \sum_{i=1}^{layers} \rho_i r_i(E,E_p) \exp\left(-\frac{(i-1)d}{\lambda_E \cos\theta_o}\right) x_i \quad (8a)$$

$$\equiv k(E,\ldots)(a_1 x_1 + a_2 x_2 + a_3 x_3 + \ldots) \quad (8b)$$

In this equation ρ_i and d may be expected to vary with composition of the alloy. Difficulties arise because $\sigma_I(E_p)$, P_A, $r_i(E,E_p)$ and λ_E might also depend upon alloy composition. The dependences of these four quantities upon composition will be referred to as matrix effects.

Progress has been made in calculating or measuring ionization cross sections,[17] backscattering factors,[10,11] Auger transition probabilities,[14] and attenuation lengths[18] in pure solids, but in

general it is difficult to calculate the absolute Auger current. In fact it is not even easy to measure the Auger current since it is superimposed upon a much larger background so that modulation techniques and a rather sophisticated analyzer must be used. Typically the peak to peak height in the derivative spectra or some appropriately integrated Auger feature is used as a measure which is taken to be proportional to the Auger intensity. Theoretical work has shown under what conditions the proportionality holds for both CMA and RFA types of Auger analyzers.[2,5] In fact, if the Auger peak shape changes (as it might with alloying or change in oxidation state) or if too large a modulation voltage is used the proportionality may break down.

To avoid many of the problems of absolute intensity measurement, it is common to use standards which provide reference intensities for calibration.

the intensities, I_E^o, from samples of the pure components prepared in

The drawback of this method is that it requires that there be no matrix effects. The factors $\sigma_I(E_p)$ and P_A might be expected to be independent of matrix

The escape depth λ_E is taken as independent of composition, an approximation which is suggested by the "universal" nature of the curve shown in Fig. 3.

Other workers have attempted to use other means of calibration.[19]

Typical methods include sputtering, scribing, or cleaving of alloys in an attempt to obtain a surface which has the same composition as the bulk.

Other techniques involve depositing some species onto a substrate and comparing the Auger intensity with the amount deposited as measured by some other means such as with a quartz crystal oscillator[20] or by ellipsometry,[9] or by radio-isotope counting techniques.

The necessary information that must be available from the experiments for quantitative analysis of the surface composition are the intensitites of each of the Auger peaks in the spectrum

and the corresponding intensities in the reference samples. To cancel the effects of instrumental drift and for purposes of normalization, these are always measured as ratios.

Two types of ratios are of use. The ratio of the intensity of a peak at an energy E divided by the intensity of the same peak in the pure reference will be denoted as ξ_E. The ratio of the intensity of a peak at an energy E to another peak at energy E' will be refered to as $R_{E/E'}$. This ratio may be measured from one sample or from one or both pure references in which case the superscript ^{o} in $R^o_{E/E'}$ will denote that the ratio is for the pure reference. Summarizing, the following definitions are given:

$$R_{E/E'} = I_E/I_{E'} \tag{9a}$$

$$R^o_{E/E'} = I^o_E/I^o_{E'} \tag{9b}$$

$$\xi_E = I_E/I^o_E \tag{9c}$$

These ratios are all measured experimentally. The $R_{E/E'}$ types of ratios are the easiest to measure since only one sample is involved. If E and E' refer to Auger transitions from the same component, then $R^o_{E/E'}$ is also easy to measure. The ratios ξ_E and $R^o_{E/E'}$ (when E and E' derive from different components) are harder to measure since at least two samples must be prepared and positioned in turn in front of the analyzer.

It is possible to calculate ξ_E. Using Eqs. 7, 8 and 9 it follows that:

$$\xi_E = \frac{k(E,\ldots)(a_1x_1 + a_2x_2 + \ldots)}{k^o(E,\ldots)(a^o_1 + a^o_2 + a^o_3 + \ldots)} \tag{10}$$

To calculate ξ_E, we substitute the proper values for k, k^o, a_i, a^o_i and the depth distribution, i.e. the compositions in each layer, x_i. The depth distribution of composition can be extracted from the experimental values of $R_{E/E'}$, $R^o_{E/E'}$, and ξ_E.

The composition layer by layer can be obtained from this data in two ways. One may suggest hypothetical depth distributions which are then used to calculate the intensity ratios. These ratios are then compared with the experimental results and the depth distribution varied to give the best fit. An alternate method is to use the experimental data to directly calculate the depth distribution.

To use Eq. 10 several assumptions are made. The first assumption is that ionization cross sections, Auger transition probabilities and the instrumental factors remain constant and are independent of composition. This assumption implies that:

$$I_p \sigma_I^o(E_p) P_A^o(\Omega/4\pi) T = k^o(E,\ldots) = k(E,\ldots) = I_p \sigma_I(E_p) P_A(\Omega/4\pi) T \qquad (11)$$

The second assumption is that below some depth the composition of each layer becomes equal to the bulk composition x_b. The Auger intensity obtained from below that depth can be summed to give an expression of the following form:

$$\xi_E = \frac{(a_1 x_1 + a_2 x_2 + \ldots + a_{k-1} x_{k-1} + a_b x_b)}{(a_1^o + a_2^o + a_3^o + \ldots)} \qquad (12)$$

From Eq. 8 and using the properties of a geometric series it can be seen that:

$$a_i = \rho_i r_i \exp\left(- \frac{(i-1)d}{\lambda_E \cos_o}\right) \qquad \text{(for } i < k) \qquad (13a)$$

$$a_b = \rho_b r_b \sum_{i=k}^{\text{layers}} \exp\left(- \frac{(i-1)d}{\lambda_E \cos\theta_o}\right) = \rho_b r_b \frac{\exp(-(k-1)d/\lambda_E \cos\theta_o)}{1 - \exp(-d/\lambda_E \cos\theta_o)} \qquad (13b)$$

From Eq. 7 it is seen that if the pure solid has the same value of ρ^o, r^o and d^o in each layer then

$$\sum_{i=1}^{\text{layers}} a_i^o = \sum_{i=1}^{\text{layers}} \rho_i^o r_i^o \exp\left(-\frac{(i-1)d^o}{\lambda_E \cos\theta_o}\right) = \rho^o r^o / \left(1 - \exp(- \frac{d^o}{\lambda_E \cos\theta_o})\right) \qquad (14)$$

It is now possible to write out an expression for the Auger intensity ratio ξ_E, in terms of contributions from each layer. This is performed by substituting Eqs. 14 and 13 into 12. For example, Au, Ag and Au-Ag alloys have nearly identical lattice parameters (within .25%) and have the same crystal structures. Therefore, $\rho_i = \rho^o_{Au} = \rho^o_{Ag} = \rho_{alloy}$. For the (111) crystal face, each plane is separated by 2.35 Å, and the values of the escape depths λ_E for various energies can be obtained from Fig. 3. The intensity values ξ_E for a hypothetical composition profile can be obtained from the equations shown in Table 1. It is assumed arbitrarily that the fourth and all deeper layers have the bulk composition. The energies E = 71, 241, 2024 and 356 eV correspond to transitions in the Auger spectrum of Au-Ag alloys

It is seen from Table 1 that for a low energy Auger transition at 71 eV, about 55% of the signal comes from the top monolayer, while for a higher energy Auger peak at 2024 eV only about 10% of the signal comes from the top layer. For this high energy transition, as much as 73% of the signal comes from deeper than the third layer. The principle uncertainty in these equations, within the framework of the model, are the values for the escape lengths λ_E, and a lack of knowledge of the form or magnitude of r and r^o.

Now that the values of ξ_E can be calculated, it is easy to calculate values for the normalized intensity rations $R_{E/E'}$ / $R^o_{E/E'}$ by using Eq. 15 given below.

Table 1. Auger intensities for Au-Ag alloys.

ρ_i = .139 atoms/Å^2

d = 2.35 Å

$\cos\theta_0$ = .740

λ_{71} = 4 Å

λ_{241} = 6 Å

λ_{356} = 8 Å

λ_{2024} = 30 Å

$$\xi_{71} = [.548\ X_1 + .248\ X_2 + .112\ X_3 + .092\ X_b][r(71eV,E_p)/r^0(71eV,E_p)]$$

$$\xi_{241} = [.471\ X_1 + .249\ X_2 + .132\ X_3 + .148\ X_b][r(241eV,E_p)/r^0(241eV,E_p)]$$

$$\xi_{356} = [.328\ X_1 + .220\ X_2 + .148\ X_3 + .304\ X_b][r(356eV,E_p)/r^0(356eV,E_p)]$$

$$\xi_{2024} = [.101\ X_1 + .090\ X_2 + .081\ X_3 + .728\ X_b][r(2024eV,E_p)/r^0(2024eV,E_p)]$$

$$R_{E/E'} \ / \ R^{o}_{E/E'} \equiv R/R^{o}_{E/E'} = \xi_E/\xi_{E'} \qquad (15)$$

which follows directly from Eq. 9. The ratios $R_{E/E'}$ and $R^{o}_{E/E'}$ (like the values I_E and I^{o}_{E}) can not be calculated without knowledge of all the factors in Eq. 7 and 8.

It should be noted that in Eq. 12 if $x_1 = x_2 = x_3 = \ldots = x_b$ and if $a_i = a^{o}_{i}$, then $\xi_E = x_b$ and similarly $R/R^{o}_{E/E'}$ is equal to the ratio of the bulk atom fractions of the components associated with the Auger peaks at E and E'.

The model provided above takes into full account attenuation of Auger electrons and it has capability of including backscattering effects as well.

Calibration of Monolayer Coverage by AES

Application to Carbon on Platinum.

A simple technique to utilize the Auger spectrum to determine the coverages and growth mechanisms of deposits is described below. This method consists of plotting the Auger peak-to-peak signal intensity from the substrate against the similar signal from the adsorbate. This technique enables one to study the growth of deposits of any adsorbate-substrate system. We apply this method to the calibration of coverage of carbon deposits on platinum.

It has been shown by various investigators[21-24] that plotting the AES peak heights of the substrate and of the adsorbate as a function of time of deposition permits the determination of the formation of a monolayer, as well as the growth mechanism. On Fig.7 we have plotted such curves for a layer-by-layer growth mechanism.[21-23] In the figure, I_{S_n} is the peak-to-peak intensity of the Auger signal due to the substrate covered with n layers of adsorbate) I_{S_o} is the Auger signal intensity due to n layers of adsorbate.

This model has been treated extensively by various authors. Let us define $\alpha^A_S = \frac{I_{S_1}}{I_{S_o}}$ as the coefficient of attenuation of the substrate Auger peak due to the presence of a monolayer of adsorbate.

Then we have the equations,

$$I_{S_n} = I_{S_o} (\alpha^A_S)^n \qquad (16)$$

and

$$I_{A_n} = I_{A_1}(1-(\alpha^A_A)^n)/(1-\alpha^A_A) \qquad (17)$$

where α^A_A is the coefficient of attenuation of the adsorbate Auger peak through a monolayer of adsorbate.

Therefore, in the case of a layer-by-layer growth mechanism, the plot of the Auger peak intensity versus coverage (or time of deposition if the sticking coefficient is constant) yields straight lines with changeing slopes (on account of the changing n value). If the sticking coefficient is constant from layer to layer, in themodel described above, the x axis of figure 6 can be either the time of deposition or ocverage. Between the breaks on the plot we have straight lines (see Figure 7) thus, the coverage is proportional to the increase of the adsorbate Auger signal and to the decrease of the substrate Auger

signal with a coefficient of proportionality changing from layer to layer. During the formation of the first layer :

$$\theta_o^1 = I_A / I_{A_1} = (I_S - I_{S_o}) / (I_{S_1} - I_{S_o}) \quad (18a)$$

where θ_o^1 is the coverage in the first layer , and I_A and I_S are the Auger peak intensities corresponding to this coverage.

Similarly $$\theta_1^2 = 1 + \frac{I_A - I_{A_1}}{I_{A_2} - I_{A_1}} = 1 + \frac{I_S - I_{S_1}}{I_{S_2} - I_{S_1}} \quad (18b)$$

where θ_1^2 is the coverage in the second layer.

We can generalize these formulae (18a,18b) for the formation of the nth layers,

$$\theta_{n-1}^n = n - 1 + \frac{I_A - I_{A_{n-1}}}{I_{A_n} - I_{A_{n-1}}} = n - 1 + \frac{I_S - I_{S_{n-1}}}{I_{S_n} - I_{S_{n-1}}} \quad (18c)$$

where θ_{n-1}^n is the coverage in the nth layer.

If we write $I_A = I_{A_{n-1}} + \Delta I_A$, where ΔI_A is the increase of the Auger peak intensity due to the adsorbate during the formation of the nth layer, and use relations (17) to calculate $I_{A_n} - I_{A_{n-1}}$, equation 3c becomes:

$$\theta_{n-1}^n = n - 1 + \frac{\Delta I_A}{(\alpha_A^A)^{n-1} I_{A_1}} \quad (19)$$

The breaks that are seen in Figure 7 are only discernible if the sticking coefficient is constant. For changing values of the sticking coefficient with coverage the curves would be smooth and would not display the breaks when a monolayer is completed.

Changes in the Auger signal intensities upon the completion of a monolayer can be seen more dramatically if <u>we plot the substrate Auger peak intensity, against the adsorbate Auger peak intensity</u>. The information displayed in Figure 7 is replotted in this new form in Figure 8.

The general shape of the curve, the position, and the number of breaks give us the following information:

1- The general shape yields the growth mechanism. In figure 8 we have shown three cases. One curve is obtained for a layer-by-layer growth mechanism (or Franck-Van der Merwe mechanism). The second curve is obtained for the growth of crystallites on top of a monolayer (or Stranski-Krastanov mechanism). The last curve is obtained for the growth of crystallites directly on the substrate (or Volmer-Weber mechanism). The number of breaks determines the nature of the growth mechanism. If there is no break in the curve, the growth is the Volmer-Weber type. If there is one break it is a Stranski-Krastanov type, and if there are several breaks it is a Franck-Van der Merwe type.

2- The first break indicates the formation of the first monolayer. The ratio I_{A_1}/I_{S_1} of the Auger peak intensities of the adsorbate an of the substrate is characteristic of the completion of the first monolayer.

3- From equation 16 , one can calculate the attenuation factor $\alpha_S^A = \frac{I_{S_1}}{I_{S_0}}$ for the Auger transitions that are utilized in this study. Similarly from equation 17 , with n=2, we deduce: $\alpha_A^A = \frac{I_{A_2}}{I_{A_1}} - 1$.

Knowing the attenuation factors we can deduce the inelastic mean free path (imfp) of the electrons through layers of adsorbate. This relation is deduced from reference23:

$$\alpha = \exp(-1/0.74\lambda) \tag{20}$$

where λ is the inelastic mean free path.

4- Knowing the parameters I_{A_1}/I_{S_1} and α_S^A, we can deduce using equation 18a a relation giving Θ_o the coverage in the first layer as a function of these parameters and of the Auger peak intensities of the adsorbate and substrate at this coverage.

$$\Theta_o^1 = \left(1 + \frac{I_S}{I_A}\frac{I_{A_1}}{I_{S_1}}\alpha_S^A - \alpha_S^A\right)^{-1} \tag{21}$$

Application to the Adsorption of Carbon on the Stepped Platinum [6(111)x(100)] Crystal Face.

We have used this technique to calibrate the carbon coverage on a stepped platinum surface Pt(s)-[6(111)x(100)].[25] These experiments have been carried out in a LEED-Auger system with a retarding grid analyzer.[25] After cleaning the crystal by argon sputtering, heating in low pressure of oxygen and flashing, we have monitored the carbon peak at 272eV and two of the platinum peaks at 64ev and 237eV. For the sake of simplicity we have plotted the Auger peak to peak signal intensity from the second derivative spectrum. The change in the peak shape might be taken into consideration in order to have an accurate calibration; our results show that, at least at our precision of measurement assuming that the peak shape does not change with coverage, is a good enough approximation.

The carbon was deposited by decomposing CO by the Auger primary electron beam . No oxygen adsorption has been noticed during these experiments. We have made runs at 300°C and at 800°C and the results are shown in figure 9.

The curve obtained at low temperature exhibits a sharp break, while the curve obtained at the higher temperature shows a much less pronounced break.

Using the model described in the previous section, we can deduce the following informations:

1- We have two different growth mechanisms; at low temperature it is a Stranski-Krastanov type, and at high temperature the Franck-Van der Merwe mechanism.

2- We can calculate the ratio I_{A_1}/I_{S_1} corresponding to the monolayer

for both experiments and at two energies of the Auger peak of platinum (see table 2).

3- We can calculate the attenuation factors, and the inelastic mean free path of the electrons corresponding to the Auger transitions of the platinum and of the carbon through the graphite layer (see table 2).

4- We deduce the equation yielding the coverage in the first monolayer for the platinum 237eV and the carbon 272eV Auger transitions,

$$\theta_o' = \left(0.4 + 1.98\,\frac{I_{Pt_{237}}}{I_{C_{272}}}\right)^{-1}$$

Determination of Oxygen Coverages[26]

We have applied this method to the calibration of oxygen on a Pt(S)-[6(111)x(100)] surface. The 64 eV and 237 eV Auger peak-to-peak signal intensities of platinum were monitored as a function of the 510 eV Auger peak-to-peak signal intensity from the oxygen while heating the crystal at 800°C in $5x10^{-7}$ Torr of oxygen. The position of the break indicates that the formation of a monolayer of oxygen occurs at $O_{510}/Pt_{64} = 0.11$ and $O_{510}/Pt_{237}=0.5$.

The LEED structure observed at the formation of an oxygen monolayer was (3-1/2 x 3-1/2)-R30°. A simple model giving rise to this structure will place one adsorbed oxygen atom on the surface for every three platinum surface atoms. Based on this model the ratio $O_{510}/Pt_{237} = 0.5$ corresponds to about $5x10^{14}$ atoms of oxygen/cm^2.

The Auger peak-to-peak signal intensity from the oxygen is proporational to the amount of adsorbed oxygen during the formation of the first monolayer. However, the ratio O_{510}/Pt_{237} is not proportional to the coverage because of the attenuation of the platinum Auger peak-to-peak signal intensity by the adsorbed oxygen. The 237 eV platinum Auger transition is attenuated by 26% during the formation of a monolayer of oxygen. Taking this factor into consideration we obtain the following relation,

$$\theta = [0.26 + 0.37\ Pt_{237}/O_{510}]^{-1}$$

where $\theta = 1$ corresponds to one oxygen atom for every three platinum surface atoms or 5×10^{14} oxygen atoms/cm^2.

Our calibration is in fairly good agreement with others[27] considering that the orientation of the surfaces, the temperature of adsorption, and the type of AES analyzer used were different.

Detection of the Oxidation State of Surface Atoms by AES

One of the most promising applications of Auger spectroscopy is in the detection of the oxidation state of surface atoms using the chemical shift of the Auger electron binding energies from emissions that involve only core levels.[28] These atomic states have narrow energy distributions. Therefore, Auger transitions that are between these inner shell states are well characterized in energy. Changes in electron binding energies that are the result of changing oxidation states of surface atoms may cause 2-10 eV shifts in these Auger electron emissions that can be correlated with formal oxidation states of atoms at the surface. This type of analysis has been used to characterize a variety of metal oxides to study the oxidation of metals.

Auger electron emissions that involve electrons from the valence band can also be used to study changes of oxidation states of surface atoms.[29] In this circumstance the shape of the Auger emission can fingerprint changes in bonding. For example, the Auger peaks from carbon deposited on the surface has a very different shape than the Auger peak from carbides. This latter peak is also referred to as carbidic carbon. There are many instances indeed when the peak shape can be used to identify certain adsorbate bonding types.

Depth Concentration Profile Analysis

When chemical analysis is desired in the near surface region, AES may be combined with ion sputtering to obtain a depth profile analysis of the composition. Using high energy ions, the surface is sputtered away layer by layer while, simultaneously, AES analysis detects the composition in depth. Sputtering rates of 100 Å/min are usually possible and the depth resolution of the composition is about 10 Å, which is mainly determined by the statistical nature of the sputtering process. In our example we show the Auger depth profile of Si thin films (∿200 Å) deposited in vacuum onto a graphite substrate.[30] As is apparent from Figure 10, carbon diffused deeply into the silicon film, and also silicon diffused into the carbon substrate during the deposition.

The Possibility of Electron Beam Induced Chemical Changes

An important concern in the application of electron scattering to probe the structure, composition, and oxidation states of surface atoms is the possibility of damage or chemical changes introduced by the incident electrons or photons. It appears that the energy density (energy/cm^3) that is deposited per unit time determines, to a large extent, the probability of "radiation damage." Incident photons appear to be less damaging than incident electrons of the same flux and energy on account of their much lower scattering cross sections and, therefore, greater depth penetration. The radiation damage probability also depends on the ability of the excited surface atom or ion to transfer its excess energy to neighbor atoms rapidly before desorption or other chemical bond-breaking processes are to occur. In fact, electron-stimulated desorption of adsorbed atoms and molecules is commonly observed and

studied. Adsorbed monolayers on metal surfaces seem to undergo rapid de-excitation via the substrate and are less susceptible to radiation damage than monolayers on insulator surfaces. The surfaces of ionic crystals are sensitive to electron beam-induced decomposition. Organic adsorbates are resistant to electron bombardment if they possess conjugated Π electron systems (aromatic molecules, phthalocyanines), which apparently aids their de-excitation. Saturated organic adsorbates, the paraffins, for example, are readily desorbed by the incident electron beams.

It is necessary to carry out electron scattering experiments using as low intensity beams as possible in order to minimize the possibility of radiation damage.

References

1. F.J. Szalkowski and G.A. Somorjai, Adv. High Temp. Chem. 4, 137 (1971).
2. C.C. Chang, Surf. Sci. 25, 53 (1971).
3. A.J. Dekker, in Solid State Physics, 6, Acad. Press, NY, 1958.
4. C.R. Brundle, Surf. Sci. 48, 99 (1975).
5. N.J. Taylor, Rev. Sci. Inst. 40, 792 (1969).
6. H. Hafner, J.A. Simpson, and C.E. Kuyatt, Rev. Sci. Inst. 39, 33 (1968).
7. P.W. Palmberg, G.K. Bohn, and J.C. Tracy, App. Phys. Lett. 15, 257 (1969).
8. S.H. Overbury, Ph.D. Thesis, Univ. of California, Berkeley, 1976.
9. F. Meyer and J.J. Vrakking, Surf. Sci. 33, 271 (1972.
10. H.E. Bishop and J.C. Riviere, J. Appl. Phys. 40, 1740 (1960).
11. D.M. Smith and T.E. Gallon, J. Phys. D. App. Phys. 7, 151 (1974).
12. D.M. Zehner, J.R. Noonan, and L.H. Jenkins, Sol. State Commun. 18, 483 (1976).
13. F. Meyer and J.H. Vrakking, Surf. Sci. 45, 409 (1974).
14. W. Bambynek, et al. Rev. Mod. Phys. 44, 716 (1972).
15. P.H. Holloway, J. Electron Spectr. I, 215 (1975.
16. J.R. Noonan, D.M. Zehner, and L.H. Jenkins, J. Vac. Sci. Technol. 13, 183 (1976).
17. M. Geyzinski, Phys. Rev. 138, A336 (1965).
18. C.J. Powell, Surf. Sci. 44, 29 (1974).
19. M.P. Seah, Surf. Sci. 40, 595 (1973).
20. L.L. Levenson et al., J. Vac. Sci. Technol. 9, 6[illegible]8 (1972).
21. T.E. Gallon, Surf. Sci. 17, 486 (1969).
22. D.C. Jackson, T.E. Gallon, and A. Chambers, Surf. Sci. 36, 381 (1973).
23. M.P. Seah, Suf. Sci. 32, 703 (1972).
24. J. Perdereau, J.P. Biberian, and G.E. Rhead, J. Phys. F : Metàl 4., 798 (1974).
25. J.P. Biberian and G.A. Somorjai, Appl. of Surf. Sci. 2, 352 (1979).
26. C.E. Smith, J.P. Biberian, and G.A. Somorjai, J. Catal. 57, 426 (1979).
27. H.P. Bonzel and R. Ku, Surf. Sci. 40, 85 (1973).
28. G.A. Somorjai, J. Chem. Phys. 56, 6097 (1972).
29. F.J. Szalkowski, P.A. Bertrand, and G.A. Somorjai, Phys. Rev. B 9,3369 (1974).
30. C. Chang and W.J. Siekhaus, J. App. Phys. 46, [illegible]02 (1975).

Figure Captions

Fig.1 Scheme of the Auger electron excitation and emission processes.

Fig.2 An experimental number of scattered electrons of energy N(N/E) versus electron energy E curve.

Fig.3 The universal curve for the electron mean free path as a function of electron kinetic energy. Dots indicate individual measurements.

Fig.4 Comparison of the retarding field and the cylindrical mirror types of Auger analyzers.

Fig.5 Comparison of Auger spectra of an Au-Ag alloy obtained with retarding field and cyclindrical mirror types of Auger analyzers.

Fig.6 Typican Auger spectra from pure gold to alloys and pure silver.

Fig.7 Schematic presentation of the Auger peak intensitites of the substrate and of the adsorbate as a function of coverage (or time of deposition) in a layer-by-layer growth mechanism.

Fig.8 Plot of the substrate Auger peak intensity as a function of the adsorbate Auger peak intensity.

Fig.9 Plot of the platinum 64 eV Auger peak intensity (upper curves) and of the platinum 237 eV Auger peak intensity (lower curves) as a function of the carbon 272 eV Auger peak intensity at two different temperatures.

Fig.10 Auger depth profile for silicon films deposi on pyrolytic graphite.

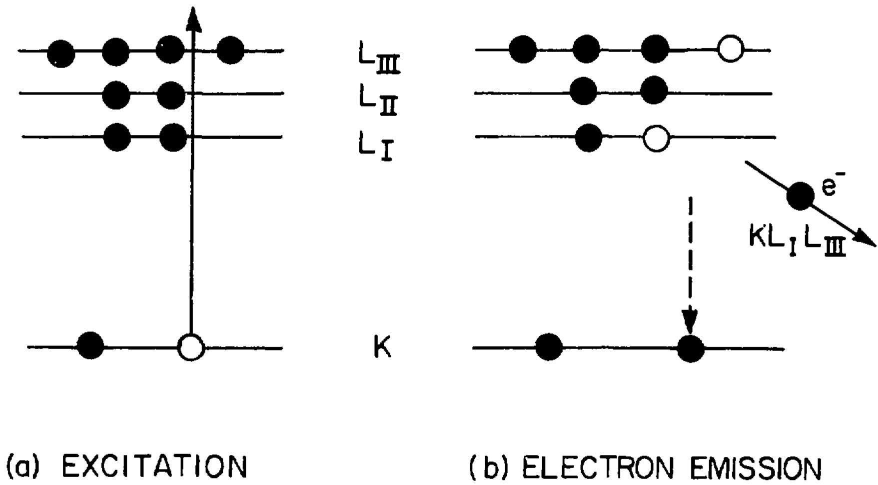

Fig.1

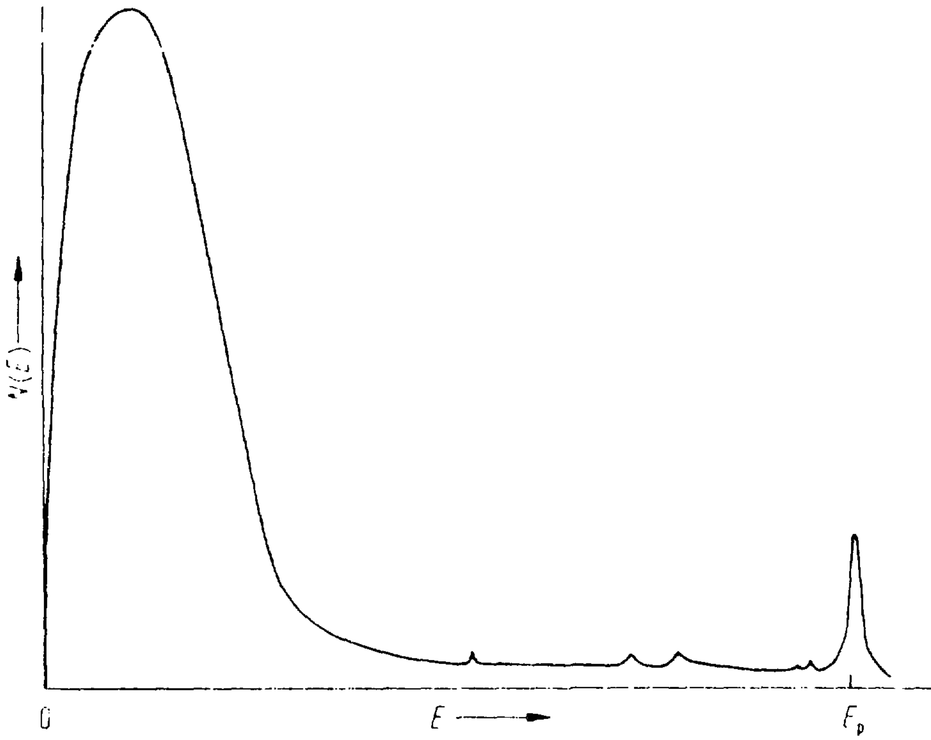

Fig.2

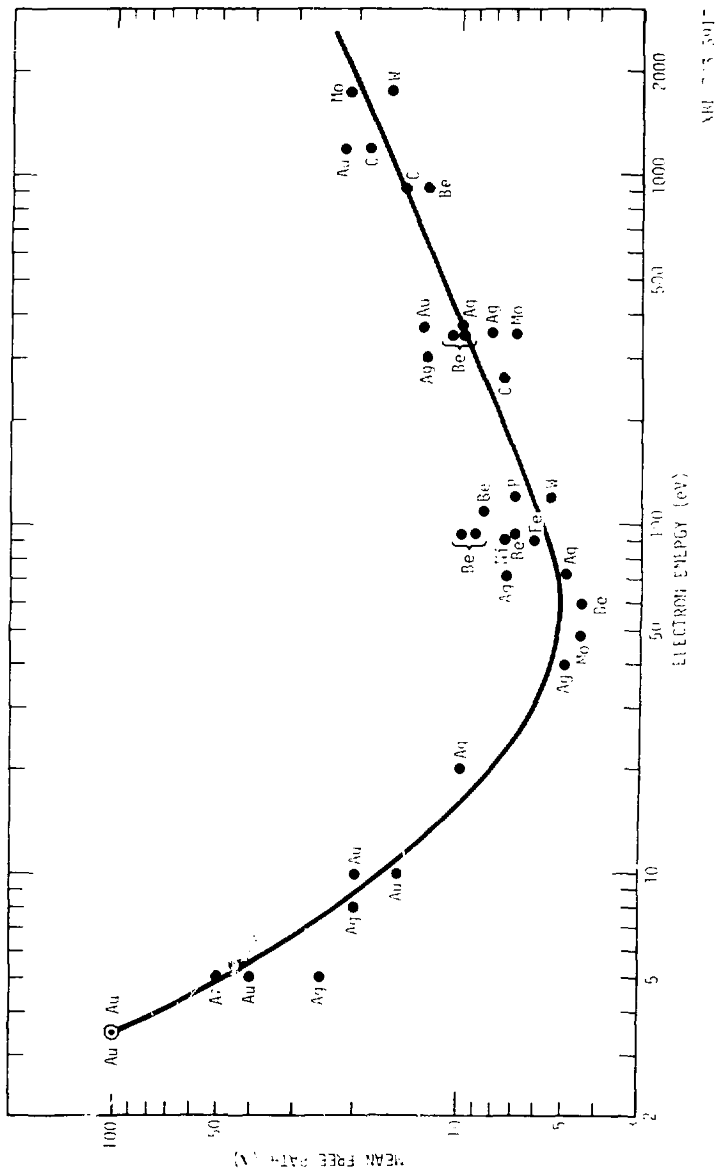

Fig. 4

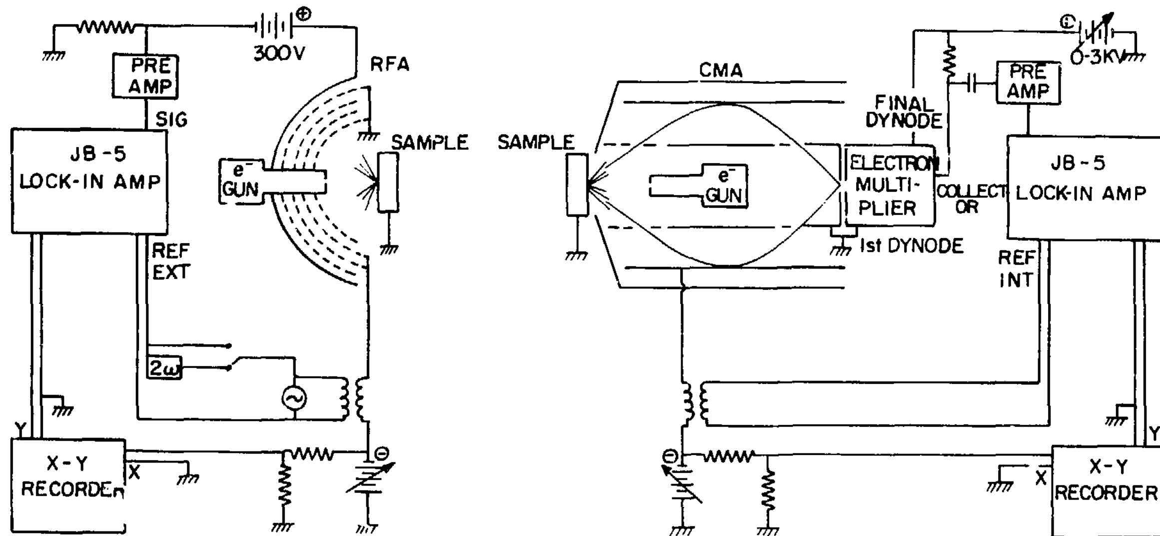

Fig.4

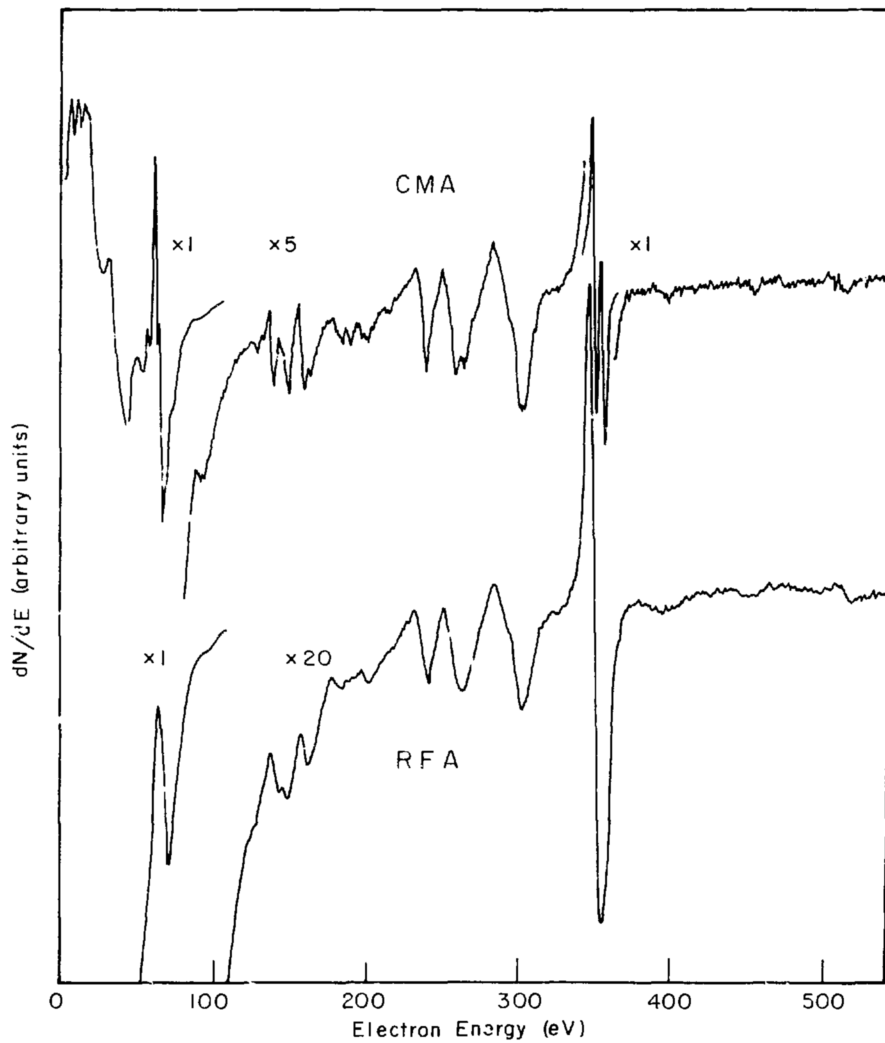

Fig.5

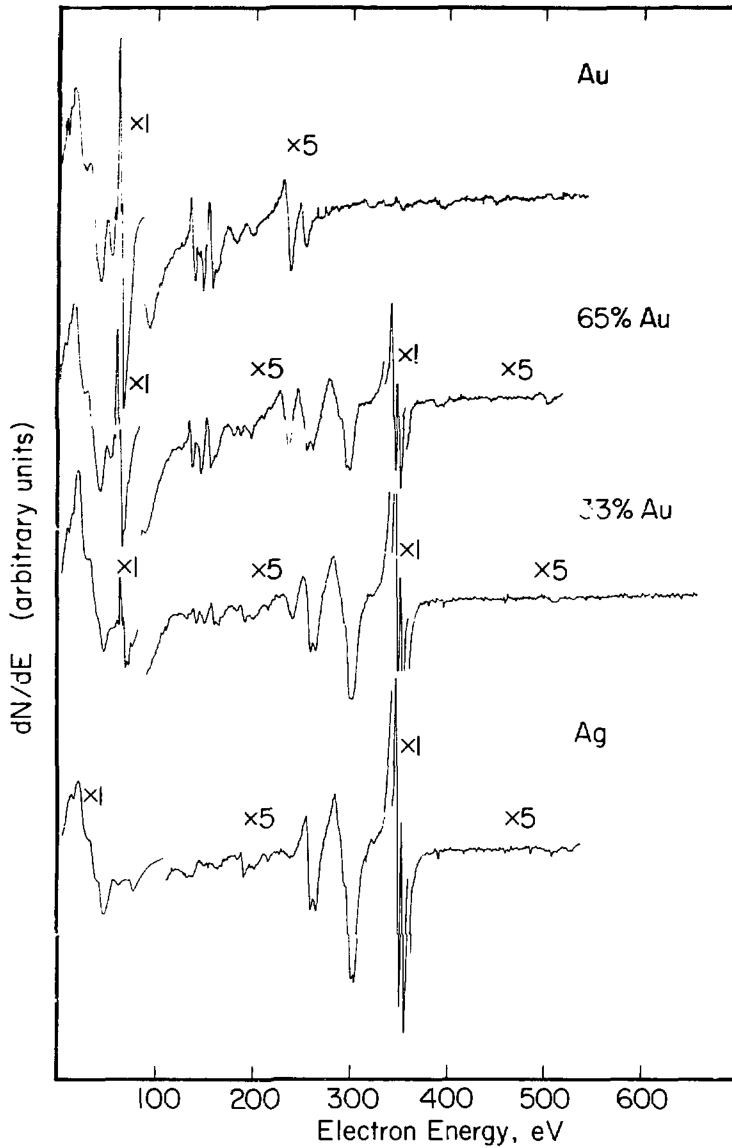

Fig.6

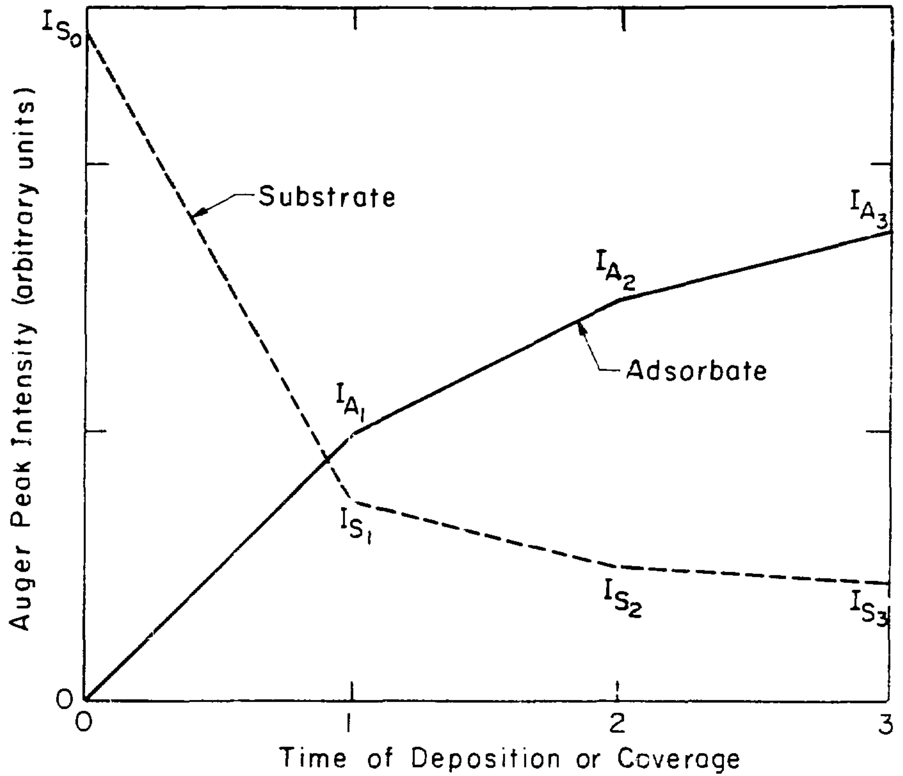

Fig.7

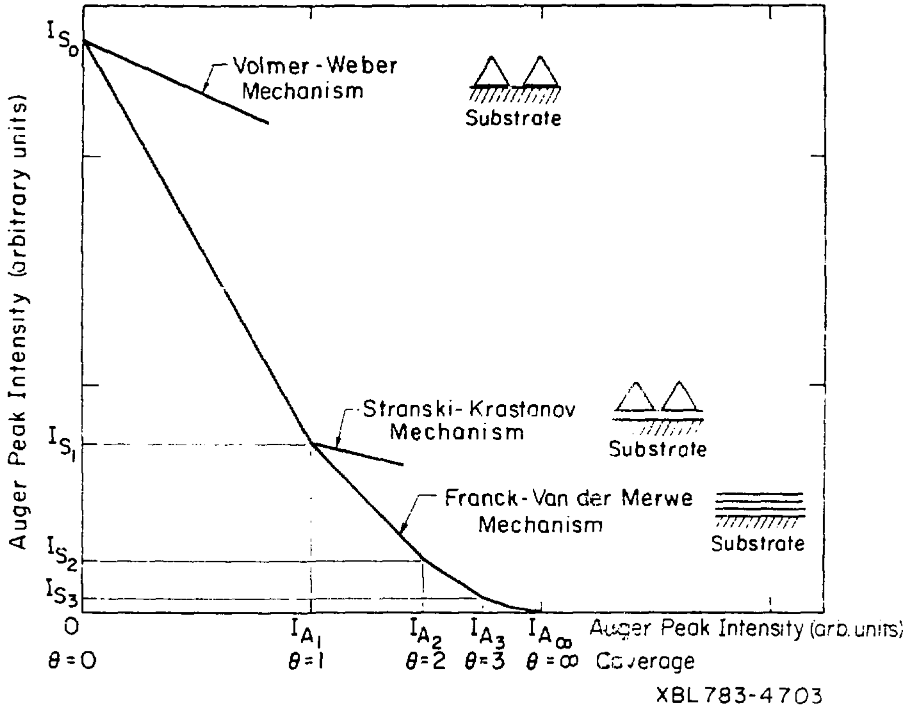

Fig.8

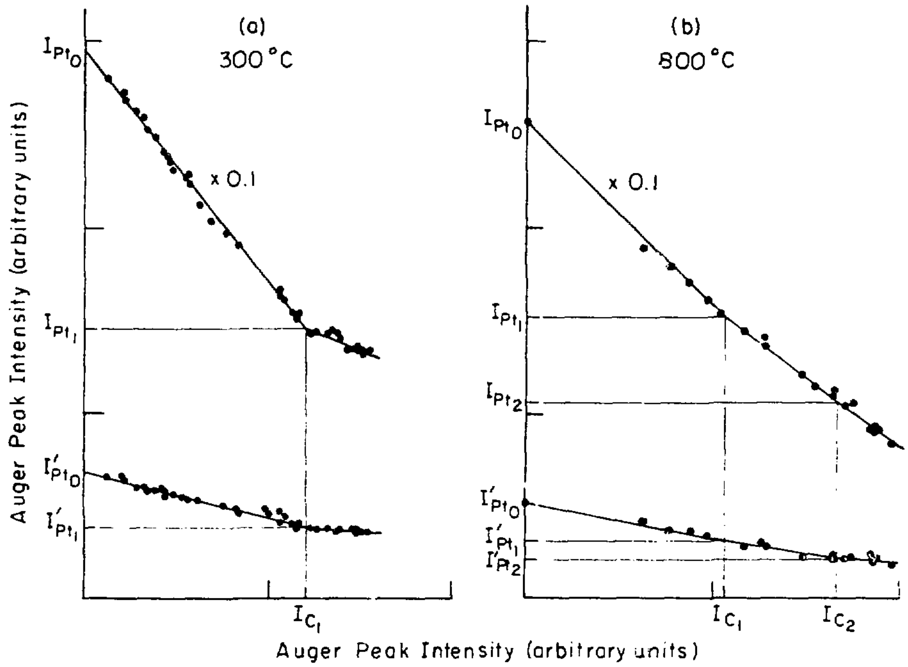

Fig.9

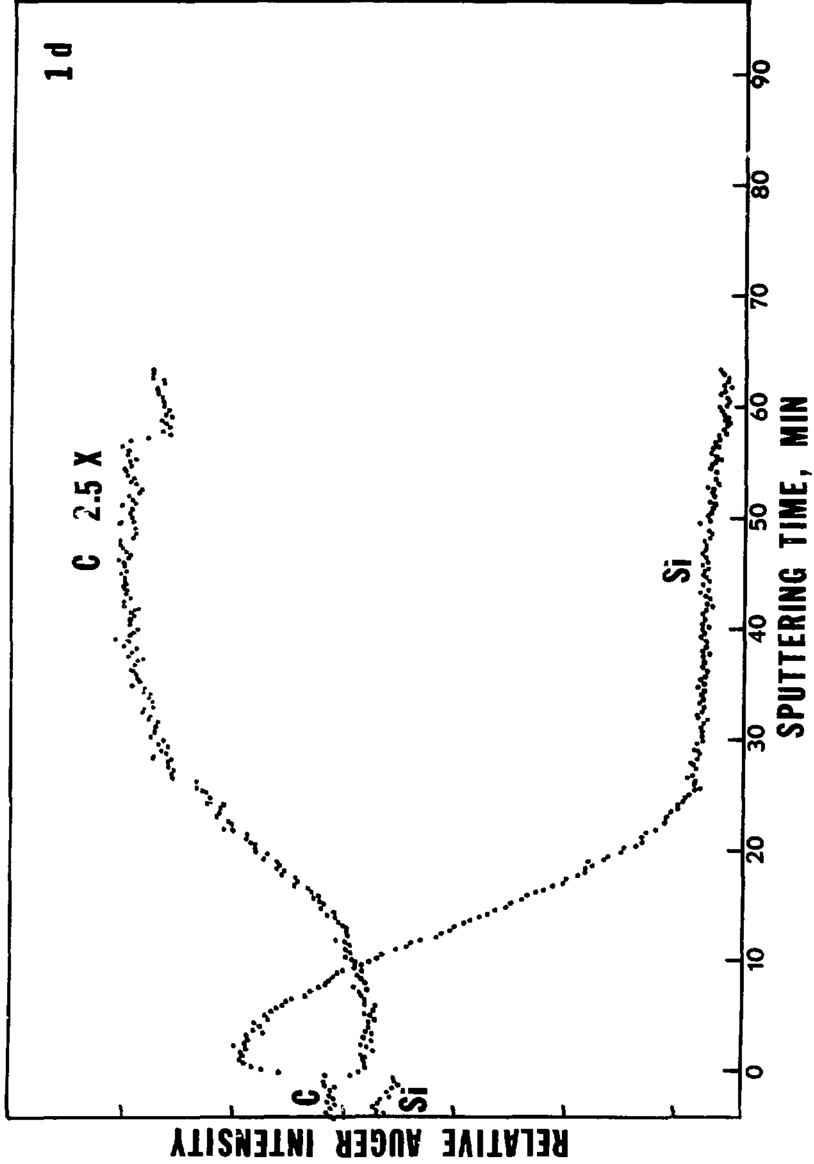

XBL 749-7320

Fig. 10